Limits on τ Lepton-Flavor Violating Decays in Three Charged Leptons

J. P. Lees,[1] V. Poireau,[1] E. Prencipe,[1] V. Tisserand,[1] J. Garra Tico,[2] E. Grauges,[2] M. Martinelli[ab,3] A. Palano[ab,3]
M. Pappagallo[ab,3] G. Eigen,[4] B. Stugu,[4] L. Sun,[4] M. Battaglia,[5] D. N. Brown,[5] B. Hooberman,[5] L. T. Kerth,[5]
Yu. G. Kolomensky,[5] G. Lynch,[5] I. L. Osipenkov,[5] T. Tanabe,[5] C. M. Hawkes,[6] N. Soni,[6] A. T. Watson,[6] H. Koch,[7]
T. Schroeder,[7] D. J. Asgeirsson,[8] C. Hearty,[8] T. S. Mattison,[8] J. A. McKenna,[8] M. Barrett,[9] A. Khan,[9]
A. Randle-Conde,[9] V. E. Blinov,[10] A. R. Buzykaev,[10] V. P. Druzhinin,[10] V. B. Golubev,[10] A. P. Onuchin,[10]
S. I. Serednyakov,[10] Yu. I. Skovpen,[10] E. P. Solodov,[10] K. Yu. Todyshev,[10] A. N. Yushkov,[10] M. Bondioli,[11]
S. Curry,[11] D. Kirkby,[11] A. J. Lankford,[11] P. Lund,[11] M. Mandelkern,[11] E. C. Martin,[11] D. P. Stoker,[11]
H. Atmacan,[12] J. W. Gary,[12] F. Liu,[12] O. Long,[12] G. M. Vitug,[12] Z. Yasin,[12] V. Sharma,[13] C. Campagnari,[14]
T. M. Hong,[14] D. Kovalskyi,[14] J. D. Richman,[14] A. M. Eisner,[15] C. A. Heusch,[15] J. Kroseberg,[15] W. S. Lockman,[15]
A. J. Martinez,[15] T. Schalk,[15] B. A. Schumm,[15] A. Seiden,[15] L. O. Winstrom,[15] C. H. Cheng,[16] D. A. Doll,[16]
B. Echenard,[16] D. G. Hitlin,[16] P. Ongmongkolkul,[16] F. C. Porter,[16] A. Y. Rakitin,[16] R. Andreassen,[17]
M. S. Dubrovin,[17] G. Mancinelli,[17] B. T. Meadows,[17] M. D. Sokoloff,[17] P. C. Bloom,[18] W. T. Ford,[18] A. Gaz,[18]
J. F. Hirschauer,[18] M. Nagel,[18] U. Nauenberg,[18] J. G. Smith,[18] S. R. Wagner,[18] R. Ayad,[19, *] W. H. Toki,[19]
E. Feltresi,[20] A. Hauke,[20] H. Jasper,[20] T. M. Karbach,[20] J. Merkel,[20] A. Petzold,[20] B. Spaan,[20] K. Wacker,[20]
M. J. Kobel,[21] K. R. Schubert,[21] R. Schwierz,[21] D. Bernard,[22] M. Verderi,[22] P. J. Clark,[23] S. Playfer,[23]
J. E. Watson,[23] M. Andreotti[ab,24] D. Bettoni[a,24] C. Bozzi[a,24] R. Calabrese[ab,24] A. Cecchi[ab,24] G. Cibinetto[ab,24]
E. Fioravanti[ab,24] P. Franchini[ab,24] E. Luppi[ab,24] M. Munerato[ab,24] M. Negrini[ab,24] A. Petrella[ab,24]
L. Piemontese[a,24] V. Santoro[ab,24] R. Baldini-Ferroli,[25] A. Calcaterra,[25] R. de Sangro,[25] G. Finocchiaro,[25]
M. Nicolaci,[25] S. Pacetti,[25] P. Patteri,[25] I. M. Peruzzi,[25, †] M. Piccolo,[25] M. Rama,[25] A. Zallo,[25] R. Contri[ab,26]
E. Guido[ab,26] M. Lo Vetere[ab,26] M. R. Monge[ab,26] S. Passaggio[a,26] C. Patrignani[ab,26] E. Robutti[a,26] S. Tosi[ab,26]
B. Bhuyan,[27] M. Morii,[28] A. Adametz,[29] J. Marks,[29] S. Schenk,[29] U. Uwer,[29] F. U. Bernlochner,[30]
H. M. Lacker,[30] T. Lueck,[30] A. Volk,[30] P. D. Dauncey,[31] M. Tibbetts,[31] P. K. Behera,[32] U. Mallik,[32] C. Chen,[33]
J. Cochran,[33] H. B. Crawley,[33] L. Dong,[33] W. T. Meyer,[33] S. Prell,[33] E. I. Rosenberg,[33] A. E. Rubin,[33]
Y. Y. Gao,[34] A. V. Gritsan,[34] Z. J. Guo,[34] N. Arnaud,[35] M. Davier,[35] D. Derkach,[35] J. Firmino da Costa,[35]
G. Grosdidier,[35] F. Le Diberder,[35] A. M. Lutz,[35] B. Malaescu,[35] P. Roudeau,[35] M. H. Schune,[35] J. Serrano,[35]
V. Sordini,[35, ‡] A. Stocchi,[35] L. Wang,[35] G. Wormser,[35] D. J. Lange,[36] D. M. Wright,[36] I. Bingham,[37] J. P. Burke,[37]
C. A. Chavez,[37] J. R. Fry,[37] E. Gabathuler,[37] R. Gamet,[37] D. E. Hutchcroft,[37] D. J. Payne,[37] C. Touramanis,[37]
A. J. Bevan,[38] F. Di Lodovico,[38] R. Sacco,[38] M. Sigamani,[38] G. Cowan,[39] S. Paramesvaran,[39] A. C. Wren,[39]
D. N. Brown,[40] C. L. Davis,[40] A. G. Denig,[41] M. Fritsch,[41] W. Gradl,[41] A. Hafner,[41] K. E. Alwyn,[42] D. Bailey,[42]
R. J. Barlow,[42] G. Jackson,[42] G. D. Lafferty,[42] T. J. West,[42] J. Anderson,[43] A. Jawahery,[43] D. A. Roberts,[43]
G. Simi,[43] J. M. Tuggle,[43] C. Dallapiccola,[44] E. Salvati,[44] R. Cowan,[45] D. Dujmic,[45] P. H. Fisher,[45] G. Sciolla,[45]
R. K. Yamamoto,[45] M. Zhao,[45] P. M. Patel,[46] S. H. Robertson,[46] M. Schram,[46] P. Biassoni[ab,47] A. Lazzaro[ab,47]
V. Lombardo[a,47] F. Palombo[ab,47] S. Stracka[ab,47] L. Cremaldi,[48] R. Godang,[48, §] R. Kroeger,[48] P. Sonnek,[48]
D. J. Summers,[48] H. W. Zhao,[48] X. Nguyen,[49] M. Simard,[49] P. Taras,[49] G. De Nardo[ab,50] D. Monorchio[ab,50]
G. Onorato[ab,50] C. Sciacca[ab,50] G. Raven,[51] H. L. Snoek,[51] C. P. Jessop,[52] K. J. Knoepfel,[52] J. M. LoSecco,[52]
W. F. Wang,[52] L. A. Corwin,[53] K. Honscheid,[53] R. Kass,[53] J. P. Morris,[53] A. M. Rahimi,[53] S. J. Sekula,[53]
N. L. Blount,[54] J. Brau,[54] R. Frey,[54] O. Igonkina,[54] J. A. Kolb,[54] M. Lu,[54] R. Rahmat,[54] N. B. Sinev,[54]
D. Strom,[54] J. Strube,[54] E. Torrence,[54] G. Castelli[ab,55] N. Gagliardi[ab,55] M. Margoni[ab,55] M. Morandin[a,55]
M. Posocco[a,55] M. Rotondo[a,55] F. Simonetto[ab,55] R. Stroili[ab,55] P. del Amo Sanchez,[56] E. Ben-Haim,[56]
G. R. Bonneaud,[56] H. Briand,[56] J. Chauveau,[56] O. Hamon,[56] Ph. Leruste,[56] G. Marchiori,[56] J. Ocariz,[56]
A. Perez,[56] J. Prendki,[56] S. Sitt,[56] M. Biasini[ab,57] E. Manoni[ab,57] C. Angelini[ab,58] G. Batignani[ab,58]
S. Bettarini[ab,58] G. Calderini[ab,58, ¶] M. Carpinelli[ab,58, **] A. Cervelli[ab,58] F. Forti[ab,58] M. A. Giorgi[ab,58]
A. Lusiani[ac,58] N. Neri[ab,58] E. Paoloni[ab,58] G. Rizzo[ab,58] J. J. Walsh[a,58] D. Lopes Pegna,[59] C. Lu,[59] J. Olsen,[59]
A. J. S. Smith,[59] A. V. Telnov,[59] F. Anulli[a,60] E. Baracchini[ab,60] G. Cavoto[a,60] R. Faccini[ab,60] F. Ferrarotto[a,60]
F. Ferroni[ab,60] M. Gaspero[ab,60] P. D. Jackson[a,60] L. Li Gioi[a,60] M. A. Mazzoni[a,60] G. Piredda[a,60] F. Renga[ab,60]
M. Ebert,[61] T. Hartmann,[61] T. Leddig,[61] H. Schröder,[61] R. Waldi,[61] T. Adye,[62] B. Franek,[62] E. O. Olaiya,[62]
F. F. Wilson,[62] S. Emery,[63] G. Hamel de Monchenault,[63] G. Vasseur,[63] Ch. Yèche,[63] M. Zito,[63] M. T. Allen,[64]
D. Aston,[64] D. J. Bard,[64] R. Bartoldus,[64] J. F. Benitez,[64] C. Cartaro,[64] R. Cenci,[64] J. P. Coleman,[64]

SLAC National Accelerator Laboratory, Menlo Park, CA 94025

M. R. Convery,[64] J. C. Dingfelder,[64] J. Dorfan,[64] G. P. Dubois-Felsmann,[64] W. Dunwoodie,[64] R. C. Field,[64]
M. Franco Sevilla,[64] B. G. Fulsom,[64] A. M. Gabareen,[64] M. T. Graham,[64] P. Grenier,[64] C. Hast,[64] W. R. Innes,[64]
J. Kaminski,[64] M. H. Kelsey,[64] H. Kim,[64] P. Kim,[64] M. L. Kocian,[64] D. W. G. S. Leith,[64] S. Li,[64]
B. Lindquist,[64] S. Luitz,[64] V. Luth,[64] H. L. Lynch,[64] D. B. MacFarlane,[64] H. Marsiske,[64] R. Messner,[64, ††]
D. R. Muller,[64] H. Neal,[64] S. Nelson,[64] C. P. O'Grady,[64] I. Ofte,[64] M. Perl,[64] B. N. Ratcliff,[64] A. Roodman,[64]
A. A. Salnikov,[64] R. H. Schindler,[64] J. Schwiening,[64] A. Snyder,[64] D. Su,[64] M. K. Sullivan,[64] K. Suzuki,[64]
S. K. Swain,[64] J. M. Thompson,[64] J. Va'vra,[64] A. P. Wagner,[64] M. Weaver,[64] C. A. West,[64] W. J. Wisniewski,[64]
M. Wittgen,[64] D. H. Wright,[64] H. W. Wulsin,[64] A. K. Yarritu,[64] C. C. Young,[64] V. Ziegler,[64] X. R. Chen,[65]
H. Liu,[65] W. Park,[65] M. V. Purohit,[65] R. M. White,[65] J. R. Wilson,[65] M. Bellis,[66] P. R. Burchat,[66]
A. J. Edwards,[66] T. S. Miyashita,[66] S. Ahmed,[67] M. S. Alam,[67] J. A. Ernst,[67] B. Pan,[67] M. A. Saeed,[67]
S. B. Zain,[67] N. Guttman,[68] A. Soffer,[68] S. M. Spanier,[69] B. J. Wogsland,[69] R. Eckmann,[70] J. L. Ritchie,[70]
A. M. Ruland,[70] C. J. Schilling,[70] R. F. Schwitters,[70] B. C. Wray,[70] J. M. Izen,[71] X. C. Lou,[71] F. Bianchi[ab],[72]
D. Gamba[ab],[72] M. Pelliccioni[ab],[72] M. Bomben[ab],[73] G. Della Ricca[ab],[73] L. Lanceri[ab],[73] L. Vitale[ab],[73] V. Azzolini,[74]
N. Lopez-March,[74] F. Martinez-Vidal,[74] D. A. Milanes,[74] A. Oyanguren,[74] J. Albert,[75] Sw. Banerjee,[75]
H. H. F. Choi,[75] K. Hamano,[75] G. J. King,[75] R. Kowalewski,[75] M. J. Lewczuk,[75] I. M. Nugent,[75] J. M. Roney,[75]
R. J. Sobie,[75] T. J. Gershon,[76] P. F. Harrison,[76] J. Ilic,[76] T. E. Latham,[76] G. B. Mohanty,[76] E. M. T. Puccio,[76]
H. R. Band,[77] X. Chen,[77] S. Dasu,[77] K. T. Flood,[77] Y. Pan,[77] R. Prepost,[77] C. O. Vuosalo,[77] and S. L. Wu[77]

(The *BABAR* Collaboration)

[1]*Laboratoire d'Annecy-le-Vieux de Physique des Particules (LAPP),*
Université de Savoie, CNRS/IN2P3, F-74941 Annecy-Le-Vieux, France
[2]*Universitat de Barcelona, Facultat de Fisica, Departament ECM, E-08028 Barcelona, Spain*
[3]*INFN Sezione di Bari[a]; Dipartimento di Fisica, Università di Bari[b], I-70126 Bari, Italy*
[4]*University of Bergen, Institute of Physics, N-5007 Bergen, Norway*
[5]*Lawrence Berkeley National Laboratory and University of California, Berkeley, California 94720, USA*
[6]*University of Birmingham, Birmingham, B15 2TT, United Kingdom*
[7]*Ruhr Universität Bochum, Institut für Experimentalphysik 1, D-44780 Bochum, Germany*
[8]*University of British Columbia, Vancouver, British Columbia, Canada V6T 1Z1*
[9]*Brunel University, Uxbridge, Middlesex UB8 3PH, United Kingdom*
[10]*Budker Institute of Nuclear Physics, Novosibirsk 630090, Russia*
[11]*University of California at Irvine, Irvine, California 92697, USA*
[12]*University of California at Riverside, Riverside, California 92521, USA*
[13]*University of California at San Diego, La Jolla, California 92093, USA*
[14]*University of California at Santa Barbara, Santa Barbara, California 93106, USA*
[15]*University of California at Santa Cruz, Institute for Particle Physics, Santa Cruz, California 95064, USA*
[16]*California Institute of Technology, Pasadena, California 91125, USA*
[17]*University of Cincinnati, Cincinnati, Ohio 45221, USA*
[18]*University of Colorado, Boulder, Colorado 80309, USA*
[19]*Colorado State University, Fort Collins, Colorado 80523, USA*
[20]*Technische Universität Dortmund, Fakultät Physik, D-44221 Dortmund, Germany*
[21]*Technische Universität Dresden, Institut für Kern- und Teilchenphysik, D-01062 Dresden, Germany*
[22]*Laboratoire Leprince-Ringuet, CNRS/IN2P3, Ecole Polytechnique, F-91128 Palaiseau, France*
[23]*University of Edinburgh, Edinburgh EH9 3JZ, United Kingdom*
[24]*INFN Sezione di Ferrara[a]; Dipartimento di Fisica, Università di Ferrara[b], I-44100 Ferrara, Italy*
[25]*INFN Laboratori Nazionali di Frascati, I-00044 Frascati, Italy*
[26]*INFN Sezione di Genova[a]; Dipartimento di Fisica, Università di Genova[b], I-16146 Genova, Italy*
[27]*Indian Institute of Technology Guwahati, Guwahati, Assam, 781 039, India*
[28]*Harvard University, Cambridge, Massachusetts 02138, USA*
[29]*Universität Heidelberg, Physikalisches Institut, Philosophenweg 12, D-69120 Heidelberg, Germany*
[30]*Humboldt-Universität zu Berlin, Institut für Physik, Newtonstr. 15, D-12489 Berlin, Germany*
[31]*Imperial College London, London, SW7 2AZ, United Kingdom*
[32]*University of Iowa, Iowa City, Iowa 52242, USA*
[33]*Iowa State University, Ames, Iowa 50011-3160, USA*
[34]*Johns Hopkins University, Baltimore, Maryland 21218, USA*
[35]*Laboratoire de l'Accélérateur Linéaire, IN2P3/CNRS et Université Paris-Sud 11,*
Centre Scientifique d'Orsay, B. P. 34, F-91898 Orsay Cedex, France
[36]*Lawrence Livermore National Laboratory, Livermore, California 94550, USA*
[37]*University of Liverpool, Liverpool L69 7ZE, United Kingdom*
[38]*Queen Mary, University of London, London, E1 4NS, United Kingdom*
[39]*University of London, Royal Holloway and Bedford New College, Egham, Surrey TW20 0EX, United Kingdom*
[40]*University of Louisville, Louisville, Kentucky 40292, USA*

^{41}Johannes Gutenberg-Universität Mainz, Institut für Kernphysik, D-55099 Mainz, Germany
^{42}University of Manchester, Manchester M13 9PL, United Kingdom
^{43}University of Maryland, College Park, Maryland 20742, USA
^{44}University of Massachusetts, Amherst, Massachusetts 01003, USA
^{45}Massachusetts Institute of Technology, Laboratory for Nuclear Science, Cambridge, Massachusetts 02139, USA
^{46}McGill University, Montréal, Québec, Canada H3A 2T8
^{47}INFN Sezione di Milano^a; Dipartimento di Fisica, Università di Milano^b, I-20133 Milano, Italy
^{48}University of Mississippi, University, Mississippi 38677, USA
^{49}Université de Montréal, Physique des Particules, Montréal, Québec, Canada H3C 3J7
^{50}INFN Sezione di Napoli^a; Dipartimento di Scienze Fisiche,
Università di Napoli Federico II^b, I-80126 Napoli, Italy
^{51}NIKHEF, National Institute for Nuclear Physics and High Energy Physics, NL-1009 DB Amsterdam, The Netherlands
^{52}University of Notre Dame, Notre Dame, Indiana 46556, USA
^{53}Ohio State University, Columbus, Ohio 43210, USA
^{54}University of Oregon, Eugene, Oregon 97403, USA
^{55}INFN Sezione di Padova^a; Dipartimento di Fisica, Università di Padova^b, I-35131 Padova, Italy
^{56}Laboratoire de Physique Nucléaire et de Hautes Energies,
IN2P3/CNRS, Université Pierre et Marie Curie-Paris6,
Université Denis Diderot-Paris7, F-75252 Paris, France
^{57}INFN Sezione di Perugia^a; Dipartimento di Fisica, Università di Perugia^b, I-06100 Perugia, Italy
^{58}INFN Sezione di Pisa^a; Dipartimento di Fisica,
Università di Pisa^b; Scuola Normale Superiore di Pisa^c, I-56127 Pisa, Italy
^{59}Princeton University, Princeton, New Jersey 08544, USA
^{60}INFN Sezione di Roma^a; Dipartimento di Fisica,
Università di Roma La Sapienza^b, I-00185 Roma, Italy
^{61}Universität Rostock, D-18051 Rostock, Germany
^{62}Rutherford Appleton Laboratory, Chilton, Didcot, Oxon, OX11 0QX, United Kingdom
^{63}CEA, Irfu, SPP, Centre de Saclay, F-91191 Gif-sur-Yvette, France
^{64}SLAC National Accelerator Laboratory, Stanford, California 94309 USA
^{65}University of South Carolina, Columbia, South Carolina 29208, USA
^{66}Stanford University, Stanford, California 94305-4060, USA
^{67}State University of New York, Albany, New York 12222, USA
^{68}Tel Aviv University, School of Physics and Astronomy, Tel Aviv, 69978, Israel
^{69}University of Tennessee, Knoxville, Tennessee 37996, USA
^{70}University of Texas at Austin, Austin, Texas 78712, USA
^{71}University of Texas at Dallas, Richardson, Texas 75083, USA
^{72}INFN Sezione di Torino^a; Dipartimento di Fisica Sperimentale, Università di Torino^b, I-10125 Torino, Italy
^{73}INFN Sezione di Trieste^a; Dipartimento di Fisica, Università di Trieste^b, I-34127 Trieste, Italy
^{74}IFIC, Universitat de Valencia-CSIC, E-46071 Valencia, Spain
^{75}University of Victoria, Victoria, British Columbia, Canada V8W 3P6
^{76}Department of Physics, University of Warwick, Coventry CV4 7AL, United Kingdom
^{77}University of Wisconsin, Madison, Wisconsin 53706, USA
(Dated: February 25, 2010)

A search for the neutrinoless, lepton-flavor violating decay of the τ lepton into three charged leptons has been performed using an integrated luminosity of $468\,\mathrm{fb}^{-1}$ collected with the BABAR detector at the PEP-II collider. In all six decay modes considered, the numbers of events found in data are compatible with the background expectations. Upper limits on the branching fractions are set in the range $(1.8 - 3.3) \times 10^{-8}$ at 90% confidence level.

*Now at Temple University, Philadelphia, Pennsylvania 19122, USA
†Also with Università di Perugia, Dipartimento di Fisica, Perugia, Italy
‡Also with Università di Roma La Sapienza, I-00185 Roma, Italy
§Now at University of South Alabama, Mobile, Alabama 36688, USA
¶Also with Laboratoire de Physique Nucléaire et de Hautes Energies, IN2P3/CNRS, Université Pierre et Marie Curie-Paris6, Université Denis Diderot-Paris7, F-75252 Paris, France
**Also with Università di Sassari, Sassari, Italy

††Deceased

Lepton-flavor violation (LFV) involving charged leptons has never been observed, and stringent experimental limits exist [1–3]. The experimental observation of neutrino oscillations [4] implies that, within the standard model (SM), there are amplitudes contributing to LFV in the charged sector, although their effects must be well below the current experimental sensitivity [5]. Many de-

scriptions of physics beyond the SM predict enhanced LFV in τ decays over μ decays with branching fractions within present experimental sensitivities [6–8]. An observation of LFV in τ decays would be a clear signature of new physics, while improved limits will further constrain models.

This paper reports the latest results from BABAR on the search for LFV in the neutrinoless decay $\tau^- \to \ell_1^- \ell_2^+ \ell_3^-$, where $\ell_i = e, \mu$ [9]. All six lepton combinations consistent with charge conservation are considered. The analysis is based on data recorded by the BABAR [10] detector at the PEP-II asymmetric-energy e^+e^- B factory operated at the SLAC National Accelerator Laboratory. The data sample is provided by an integrated luminosity of $426\,\mathrm{fb}^{-1}$ recorded at a center-of-mass (c.m.) energy $\sqrt{s} = 10.58\,\mathrm{GeV}$, and of $42\,\mathrm{fb}^{-1}$ recorded at about $\sqrt{s} = 10.54\,\mathrm{GeV}$. With these conditions, the expected cross section for τ-pair production is $\sigma_{\tau\tau} = 0.919 \pm 0.003$ nb [11], corresponding to a data sample of about 430 million τ-pairs.

Charged-particle (track) momenta are measured with a 5-layer double-sided silicon vertex tracker and a 40-layer helium-isobutane drift chamber inside a 1.5 T superconducting solenoid magnet. An electromagnetic calorimeter consisting of 6580 CsI(Tl) crystals is used to measure electron and photon energies, a ring-imaging Cherenkov detector is used to identify charged hadrons, and the instrumented magnetic flux return (IFR) is used to identify muons. About half of the data sample under study was recorded with the IFR instrumented with resistive plate chambers (RPC). During the second half of the data taking period most RPCs were replaced by limited streamer tubes in the barrel section of the IFR.

A Monte Carlo (MC) simulation of lepton-flavor violating τ decays is used to estimate the signal efficiency and optimize the search. Simulated τ-pair events including higher-order radiative corrections are generated using KK2f [12] with one τ decaying to three leptons with a uniform three-body phase space distribution, while the other τ decays according to measured rates [13] simulated with Tauola [14]. Final-state radiative effects are simulated for all decays using Photos [15]. The detector response is simulated with GEANT4 [16].

The signature for $\tau^- \to \ell_1^- \ell_2^+ \ell_3^-$ is a set of three charged particles, each identified as either an e or a μ, with an invariant mass and energy equal to that of the parent τ lepton. Events are preselected requiring four reconstructed tracks and zero net charge, selecting only tracks pointing toward a common region consistent with $\tau^+\tau^-$ production and decay. The polar angles of all four tracks in the laboratory frame are required to be within the calorimeter acceptance range, to ensure good particle identification. The event is divided into two hemispheres in the e^+e^- c.m. frame using the plane containing the interaction point and perpendicular to the thrust axis, as calculated from the observed tracks and neutral energy deposits. The signal hemisphere must contain exactly three tracks (3-prong) with an invariant mass less than

3.5 GeV/c^2, while the other hemisphere must contain exactly one (1-prong) track, and may contain also neutral energy deposits. In order to reduce backgrounds coming from photon conversions we require that the two couples of oppositely charged tracks in the 3-prong hemisphere have an invariant mass, calculated using electron mass hypothesis for the tracks, larger than than 20 MeV/c^2, or 30 MeV/c^2 for $e^-e^+e^-$ and $e^-\mu^+\mu^-$.

With respect to our previous result [17], this analysis relies on significantly improved particle identification (PID) techniques for both $\mu^\pm$ and $e^\pm$. Electrons are identified applying a multivariate algorithm which uses as input the ratio of calorimeter energy to track momentum (E/p), the ionization energy loss in the tracking system ($\mathrm{d}E/\mathrm{d}x$), and the shape of the shower in the calorimeter. Muon identification exploits a bagged decision tree (BDT)[18] algorithm, which uses as input the number of hits in the IFR, the number of interaction lengths traversed, and the energy deposition in the calorimeter. Since $\mu^\pm$ with momenta less than 500 MeV/c do not penetrate enough into the IFR to provide useful information, the BDT also uses information obtained from the inner trackers to maintain a very low $\pi - \mu$ misidentification probability with high selection efficiencies. The electron and muon identification efficiencies are measured to be 91% and 77% respectively. The probability for a $\pi^\pm$ to be misidentified as an $e^\pm$ in 3-prong τ decays is 2.4%, while the probability to be misidentified as a $\mu^\pm$ is 2.1%.

The quantity $\Delta E \equiv E_{\mathrm{rec}}^\star - E_{\mathrm{beam}}^\star$ is defined, where $E_{\mathrm{rec}}^\star$ is the total energy of the system observed in the 3-prong hemisphere and $E_{\mathrm{beam}}^\star$ is the beam energy (the superscript $\star$ indicates quantities measured in the c.m. frame). We define $\Delta M_{ec} \equiv M_{ec} - m_\tau$ with $M_{ec}^2 \equiv E_{beam}^{\star 2}/c^4 - |\vec{p}_{3l}^\star|^2/c^2$, where $|\vec{p}_{3l}^\star|^2$ is the squared momentum of the 3-prong system, $m_\tau = 1.777\,\mathrm{GeV}/c^2$ is the τ mass [13], and the energy constrained momentum of the 3-prong system, $|\vec{p}_{3l}^\star|$, is obtained from a kinematic fit: the fit requires the τ energy measured in the c.m. to be $\sqrt{s}/2$, taking into account the errors on the reconstructed track parameters and the beam energy measurement.

The signal distributions in the ($\Delta M_{ec}, \Delta E$) plane (see Fig. 1) are broadened by detector resolution and radiative effects. In all decay modes, the radiation of photons from the incoming e^+e^- particles and from the outgoing τ decay products leads to a tail at low values of ΔE. Radiation from the final-state leptons, which is more likely for electrons than for muons, produces a tail at high values of ΔM_{ec} as well. Signal regions (SR) in the ($\Delta M_{ec}, \Delta E$) plane are optimized in order to obtain the smallest expected upper limit (UL) when no LFV signal is present. The expected ULs are estimated using MC simulations and data control samples, instead of candidate signal events. The upper right corner of the signal region in the ($\Delta M_{ec}, \Delta E$) plane, in units of (MeV/c^2, MeV), is fixed at (30,50) for $\mu^-e^+e^-$ and $e^-\mu^+\mu^-$ and at (30,100) for the other four channels. The lower left corner is at (−30,−300) for the $e^-e^+e^-$, $\mu^-e^+e^-$, and $e^-\mu^+\mu^-$ decay modes, (−30,−350)
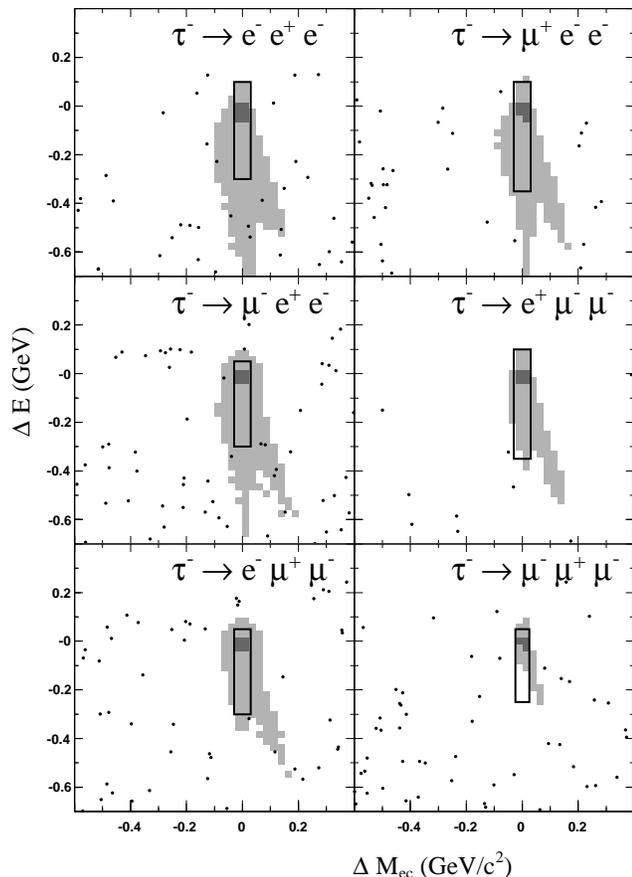
FIG. 1: Data events (dots) in the large box of the $(\Delta M_{ec}, \Delta E)$ as defined in the text, for the six τ decay channels after all selection is applied. The solid black lines are the boundaries, for each channel, of the signal region. The dark and light shadings represent the 50% and 90% signal contours respectively.

for $\mu^+ e^- e^-$ and $e^+ \mu^- \mu^-$, and $(-25, -200)$ for $\mu^- \mu^+ \mu^-$. Fig. 1 shows the observed data in the $(\Delta M_{ec}, \Delta E)$ plane, along with the signal region boundaries and the expected signal distributions. To avoid biases, a blind analysis procedure was followed, with the number of events in the SR remaining unknown until the selection criteria were finalized and all cross-checks were performed.

Each track present in the signal hemisphere must be identified as either a muon or an electron, depending on the channel under study. For the channels where two tracks of the same charge sign can be either an electron or a muon (i.e. $\mu^- e^+ e^-$ and $e^- \mu^+ \mu^-$), it is possible that both tracks satisfy both electron and muon PID selectors: in these rare cases we measure ΔM_{ec} and ΔE in both mass hypotheses. For all events showing this behavior only one of the two combinations falls in the large box (LB) of the $(\Delta M_{ec}, \Delta E)$ plane, defined as the region lying between -600 and $400 \,\mathrm{MeV}/c^2$ in ΔM_{ec} and -700 and $400 \,\mathrm{MeV}$ in ΔE.

The PID requirements strongly suppress background,

but further selection is applied: for all decay modes, the momentum of the 1-prong track is required to be less than 4.8 GeV/c in the c.m. frame. The 1-prong side τ mass is approximately reconstructed from the 4-momentum obtained by adding the 1-prong track, the neutral energy deposits in the 1-prong hemisphere, and the missing 3-momentum of the event, assuming a zero mass as is appropriate if just a single neutrino is missing. This invariant mass is required to be in the range $0.2 - 3.0 \,\mathrm{GeV}/c^2$ for $e^- e^+ e^-$, $\mu^- e^+ e^-$, and $e^- \mu^+ \mu^-$, and in the range of $0.1 - 3.5 \,\mathrm{GeV}/c^2$ for $\mu^+ e^- e^-$, $e^+ \mu^- \mu^-$, and $\mu^- \mu^+ \mu^-$. To suppress Bhabha backgrounds we reject events where any oppositely charged track pair has an invariant mass compatible with a photon conversion when assigning the electron mass to the two tracks. $M_{e^+ e^-}$ is required to be $< 200 \,\mathrm{MeV}/c^2$ for all channels except for $e^+ \mu^- \mu^-$ where $M_{e^+ e^-} < 300 \,\mathrm{MeV}/c^2$ is required. For the $e^- e^+ e^-$ and $e^- \mu^+ \mu^-$ decay modes, the charged particle in the 1-prong hemisphere is required to be matched to an energy deposit in the calorimeter inconsistent with an electron, and must not be identified as an electron, while for the $\mu^+ e^- e^-$, $\mu^- e^+ e^-$, and $\mu^- \mu^+ \mu^-$ decay modes this track must not be identified as a muon. For the $e^- e^+ e^-$ and $e^- \mu^+ \mu^-$ decay modes, the missing momentum of the event should be greater than $300 \,\mathrm{MeV}/c$, for $e^- \mu^+ \mu^-$ and $\mu^- \mu^+ \mu^-$ this should be more than $200 \,\mathrm{MeV}/c$ and for $\mu^+ e^- e^-$ and $e^+ \mu^- \mu^-$ this lower limit is set at $100 \,\mathrm{MeV}/c$. For the $e^- e^+ e^-$ and $\mu^+ e^- e^-$ channels the cosine of the angle between the direction of the sum of the three signal track momenta and the direction of the 1-prong track momentum (θ_{13}), is required to satisfy $\cos(\theta_{13}) > -0.995$ and $\cos(\theta_{13}) > -0.997$ respectively, to further reduce Bhabha contributions.

The backgrounds still contaminating the sample have been identified in three broad categories: low multiplicity $q\bar{q}$ events (comprising both continuum light quark pairs and $c\bar{c}$ pairs), QED events (Bhabha or $\mu^+ \mu^-$ depending on the particular channel), and SM $\tau^+ \tau^-$ events. These three background classes have distinctive distributions in the $(\Delta M_{ec}, \Delta E)$ plane. The $q\bar{q}$ events tend to populate the plane uniformly, while QED backgrounds fall in a narrow band at positive values of ΔE, and $\tau^+ \tau^-$ backgrounds are restricted to negative values of both ΔE and ΔM_{ec} due to the presence of at least one undetected neutrino. The possible background contribution arising from two-photon processes has been studied on a data control sample, as discussed in the following, and it is found to be negligible.

The expected background rates for each decay mode are determined by fitting a set of probability density functions (PDFs) to the observed data in the grand sideband (GS) region of the $(\Delta M_{ec}, \Delta E)$ plane as was done in the previous published analysis [17]. The GS region covers the same region as the LB but does not include the SR. The functional forms of the PDFs are the same as in [17]. For the $q\bar{q}$ background, a two-dimensional PDF is constructed from the product of two PDFs, $P_{M'}$ and $P_{E'}$, where $P_{M'}(\Delta M')$ is a bifurcated Gaussian and

$P_{E'}(\Delta E') = (1 - x/\sqrt{1 + x^2})(1 + ax + bx^2 + cx^3)$ with $x = (\Delta E' - d)/e$. The $(\Delta M', \Delta E')$ axes have been slightly rotated from $(\Delta M_{ec}, \Delta E)$ to take into account the observed correlation between ΔE and ΔM_{ec} for the distribution. For the $\tau^+\tau^-$ background PDF, the function $P_{M''}(\Delta M'')$ is the sum of two Gaussians with common mean, while the functional form of $P_{E''}(\Delta E'')$ is the same as that for the $q\bar{q}$ PDF. To properly model the wedge-shaped distribution due to the kinematic limit in tau decays, a coordinate transformation of the form $\Delta M'' = \cos\beta_1 \Delta M_{ec} + \sin\beta_1 \Delta E$ and $\Delta E'' = \cos\beta_2 \Delta E - \sin\beta_2 \Delta M_{ec}$ is performed.

QED backgrounds represent one of the major sources of backgrounds for $e^-e^+e^-$, $\mu^+e^-e^-$, $\mu^-e^+e^-$, and $e^-\mu^+\mu^-$. To study this background category, specially selected control samples obtained from data were produced. Two different methods were used to extract QED control samples: for $e^-e^+e^-$, $\mu^+e^-e^-$, and $e^-\mu^+\mu^-$ channels the sample was produced selecting events passing all selection requirements, except the lepton veto in the tag side, and requiring the track in the tag-side to be identified as a muon ($\mu^+e^-e^-$ channel) or as an electron (for the other two channels). To obtain a large enough sample for the $\mu^-e^+e^-$ channel we selected events where a muon is present in the tag-side, and the reconstructed mass in the tag-side is between $0.5\,\text{GeV}/c^2$ and $2.5\,\text{GeV}/c^2$, and the momentum of the tag-side particle is required to be larger than $4.8\,\text{GeV}/c$. To fit these control samples, an analytic PDF is constructed from the product of a Crystal Ball function [19] in $\Delta E'$ and a third-order polynomial in $\Delta M'$, where again the $(\Delta M', \Delta E')$ axes have been rotated slightly from $(\Delta M_{ec}, \Delta E)$ to fit the observed distribution.

The expected background rate in the SR is obtained by an unbinned maximum likelihood fit to the data in the GS region, with the shapes of the three background PDFs fixed by making an unbinned likelihood fit to the MC and the control samples. The PDF shape determinations and background fits are performed separately for each of the six decay modes. Cross-checks of the background estimation are performed by considering the numbers of events expected and observed in sideband regions immediately neighboring the signal region for each decay mode.

The efficiency of the selection for signal events is estimated with the MC simulation of signal LFV events. The efficiency of signal MC passing preselection requirements varies between 45% and 49%. The total efficiency for signal events to be found in the signal region is shown in Table I for each decay mode and ranges from 6.4% to 12.7%. This efficiency includes the 85% branching fraction for 1-prong τ decays. With respect to the previous analysis, improvements in particle ID, in tracking algorithms and in selection criteria allowed us to obtain higher signal efficiencies along with a reduction of the expected backgrounds thus improving the UL sensitivity.

Uncertainties in signal efficiency estimation and in the number of the expected events in the SR obtained by the fit affect the final result. The systematic uncertainties

TABLE I: Efficiencies, numbers of expected background events (N_{bgd}), expected branching fraction upper limits at 90% CL ($\text{UL}_{90}^{\text{exp}}$), numbers of observed events (N_{obs}), and observed branching fraction upper limits at 90% CL ($\text{UL}_{90}^{\text{obs}}$) for each decay mode. All upper limits are in units of 10^{-8}.

Mode	Eff. [%]	N_{bgd}	$\text{UL}_{90}^{\text{exp}}$	N_{obs}	$\text{UL}_{90}^{\text{obs}}$
$e^-e^+e^-$	8.6 ± 0.2	0.12 ± 0.02	3.4	0	2.9
$\mu^-e^+e^-$	8.8 ± 0.5	0.64 ± 0.19	3.7	0	2.2
$\mu^+e^-e^-$	12.7 ± 0.7	0.34 ± 0.12	2.2	0	1.8
$e^+\mu^-\mu^-$	10.2 ± 0.6	0.03 ± 0.02	2.8	0	2.6
$e^-\mu^+\mu^-$	6.4 ± 0.4	0.54 ± 0.14	4.6	0	3.2
$\mu^-\mu^+\mu^-$	6.6 ± 0.6	0.44 ± 0.17	4.0	0	3.3

from PID dominate the error on the efficiency. They are estimated on data control samples, looking at the discrepancies between data and MC samples, by measuring the average spread for tracks with the same kinematic properties. These uncertainties vary between a relative error of 1.8% for $e^-e^+e^-$ and 7.8% for $\mu^-\mu^+\mu^-$. The modeling of the tracking efficiency contributes an additional 1% relative uncertainty. All other sources of uncertainty in the signal efficiency are found to be smaller than 1.0%, including the statistical limitation of the MC signal samples, the modeling of higher-order radiative effects, track momentum resolution, trigger performance, observables used in the selection criteria, and knowledge of the tau 1-prong branching fractions.

The systematic uncertainty due to errors in background estimation is determined from fits to data in the GS region. In addition to varying PDF parameters by their uncertainties, alternative functional forms are used to determine the uncertainty on the expected background yield in the SR. The total errors on the background estimates are reported in Table I. Systematics coming from unsimulated background contributions, such as two-photon processes, are checked using background enriched control samples. Two-photon processes are characterized by a small transverse momentum, so the control samples were produced selecting events with a transverse momentum smaller than $0.2\,\text{GeV}/c$, and with the momentum of the tag-side track in the center of mass smaller than $4.0\,\text{GeV}/c$. The uncertainties introduced by two-photon processes and unsimulated backgrounds are found to be negligible.

Background expectations (N_{bgd}) and the number of observed events (N_{obs}) are shown in Table I. No events are observed in the SR for any of the modes and we place 90% confidence level (CL) ULs on the branching fractions using $\text{UL}_{90}^{\text{exp}} = N_{\text{UL}}^{90}/(2\varepsilon L\sigma_{\tau\tau})$, where N_{UL}^{90} is the 90% CL UL for the number of signal events when N_{obs} events are observed with N_{bgd} background events expected. The values ε, L, and $\sigma_{\tau\tau}$ are the selection efficiency, luminosity, and $\tau^+\tau^-$ cross section, respectively. The uncertainty on the product $L \cdot \sigma_{\tau\tau}$ is 0.9%. The branching fraction ULs are calculated, with all uncertainties included,

using the technique of Cousins and Highland [20] following the implementation of Barlow [21]. The expected average upper limit UL_{90}^{exp}, defined as the mean UL expected in the background-only hypothesis, is included in Table I. The 90% CL ULs on the $\tau^- \to \ell_1^- \ell_2^+ \ell_3^-$ branching fractions are in the range $(1.8 - 3.3) \times 10^{-8}$. These limits supersede the previous BABAR analysis [17], and are compatible with the latest Belle limits [22].

[1] MEGA/LAMPF Collaboration, M. L. Brooks et al., Phys. Rev. Lett. **83**, 1521 (1999).

[2] SINDRUM Collaboration, U. Bellgardt et al., Nucl. Phys. B **299**, 1 (1988).

[3] K. Inami, Nucl. Phys. B Proc. Suppl. **181-182**, 295 (2008).

[4] Homestake Collaboration, B. T. Cleveland et al., Astrophys. J. **496**, 505 (1998); K2K Collaboration, M. H. Ahn et al., Phys. Rev. Lett. **90**, 041801 (2003); KamLAND Collaboration, K. Eguchi et al., Phys. Rev. Lett. **90**, 021802 (2003); SNO Collaboration, Q. R. Ahmad et al., Phys. Rev. Lett. **89**, 011301 (2002); Super-Kamiokande Collaboration, Y. Fukuda et al., Phys. Rev. Lett. **81**, 1562 (1998).

[5] W.J. Marciano and A.I. Sanda, Phys. Lett. B **67**, 303 (1977).

[6] P. Paradisi, JHEP **0510**, 006 (2005).

[7] K. S. Babu and C. Kolda, Phys. Rev. Lett. **89**, 241802 (2002).

[8] A. Brignole and A. Rossi, Phys. Lett. B **566**, 217 (2003).

[9] Throughout this paper, charge conjugate decay modes are implied.

[10] BABAR Collaboration, B. Aubert et al., Nucl. Instrum. Methods Phys. Res., Sect. A **479**, 1 (2002).

[11] S. Banerjee, B. Pietrzyk, J. M. Roney, and Z. Was, Phys. Rev. D **77**, 054012 (2008).

[12] S. Jadach, B. F. Ward, and Z. Was, Comput. Phys. Commun. **130**, 260 (2000).

[13] Particle Data Group, Y.-M. Yao et al., J. Phys. **G33**, 1 (2006).

[14] S. Jadach, Z. Was, R. Decker, and J. H. Kuhn, Comput. Phys. Commun. **76**, 361 (1993).

[15] E. Barberio and Z. Was, Comput. Phys. Commun. **79**, 291 (1994).

[16] GEANT4 Collaboration, S. Agostinelli et al., Nucl. Instrum. Methods Phys. Res., Sect. A **506**, 250 (2003).

[17] BABAR Collaboration, B. Aubert et al., Phys. Rev. Lett. **99**, 251803 (2007).

[18] E. L. Allwein, R. E. Schapire and Y. Singer, J. Machine Learning Res. **1**, 113 (2000).

[19] J. Gaiser et al., Phys. Rev. D **34**, 711 (1986).

[20] R. D. Cousins and V. L. Highland, Nucl. Instrum. Methods Phys. Res. A **320**, 331 (1992).

[21] R. Barlow, Comput. Phys. Commun. **149**, 97 (2002).

[22] Belle Collaboration, Y. Miyazaki et al., submitted to Phys. Lett. B